AIAA JOURNAL
Vol. 38, No. 10, October 2000

Supersonic Nonequilibrium Plasma Wind-Tunnel Measurements of Shock Modification and Flow Visualization

R. Yano,* V. Contini,* E. Plönjes,† P. Palm,† S. Merriman,‡ S. Aithal,† I. Adamovich,§
W. Lempert,¶ V. Subramaniam,** and J. W. Rich††
Ohio State University, Columbus, Ohio 43220-1107

Experiments conducted in a new, small-scale, nonequilibrium plasma wind tunnel recently developed at Ohio State University are discussed. The facility provides a steady-state supersonic flow of cold nonequilibrium plasma with well-characterized, near uniform, properties. The plasma is produced in aerodynamically stabilized high-pressure glow discharge that forms the plenum of the supersonic nozzle. The possible modification of the supersonic flow due to ionization is studied by measuring the angle of oblique shocks attached to the wedge located in the nozzle test section. The results do not show any detectable shock weakening or attenuation in weakly ionized nitrogen plasma, compared to the measurements in a nonionized gas flow. Experiments in supersonic flowing nitrogen and helium afterglow also demonstrate a novel technique for high-density supersonic flow visualization. It allows identifying all key features of the supersonic flow, including shocks, boundary layers, flow separation regions, and wakes by recording intense visible radiation of the weakly ionized plasmas. Interpretation of radiation intensity distributions in nonequilibrium supersonic flowing afterglow may provide information on key mechanisms of energy storage and ultraviolet radiation in high-altitude rocket plumes. In addition, these flow visualization experiments can be used for validation of multidimensional computer flow codes used for internal flow simulation.

I. Introduction

SHOCK wave propagation in weakly ionized plasmas (ionization fraction $n_e/N \sim 10^{-8}$–10^{-6}) has been extensively studied for the last 15 years, mostly in Russia[1–11] and recently in the United States.[12,13] The following anomalous effects have been observed: 1) shock acceleration, 2) nonmonotonic variation of flow parameters behind the shock front, 3) shock weakening, and 4) shock wave splitting and spreading. These effects have been observed in discharges in various gases (air, CO_2, Ar), at pressures of 3–30 torr, and for Mach numbers $M \sim 1.5$–4.5. They also persist for a long time after the discharge is off ($\sim$1 ms in air[2,9]).

As is well known, shock wave acceleration can be qualitatively explained by gas heating in the discharge and/or by energy relaxation of the species excited in a discharge. A number of one-dimensional models have been proposed that predict acceleration of the shock traveling in a vibrationally excited gas, for example moist nitrogen, or across an axial temperature gradient.[14–16] Energy relaxation models also predict nonmonotonic variation of flow parameters behind shocks in molecular gas plasmas. However, they fail to explain why these effects occur in monatomic gases such as argon, where much less energy is stored in the internal degrees of freedom.

At this moment, we cannot rule out the possibility that the observed plasma shock effects are simply due to the distortion of a plane shock wave front propagating in a region with a transverse temperature gradient. Indeed, two-dimensional inviscid calculations[17] demonstrate this kind of distortion and the shock spreading within a heated cathode layer of a transverse pulsed discharge in air.[10] The gas temperature distribution in the experiment[10] has been measured by optical interferometry. Similar calculations[18] also showed shock dispersion by the transverse temperature gradient. However, neither of these calculations show any shock splitting outside the heated layer, in a cold plasma flow, where it has been measured experimentally.[10] It remains unclear how much the spatially inhomogeneous gas heating by a discharge contributed to the shock wave distortion in the experiments.[12,13]

At the present time, no consistent theoretical model has been advanced that explains all of the features of these various experiments. If the level of plasma heating and the magnitude of thermal gradients in these experiments are as small as reported, the plasma shock strength reduction is a strikingly unexplained result. Global gasdynamic analysis[19] indicates that transport of energy of the order of $\sim$100 W/cm^2 across the shock wave would be required to achieve the reported levels of shock wave dispersion. There is no process yet identified that can supply this flux for any of the different gas species used in the experiments.

A major complexity with previous plasma shock experiments has been the use of short-duration test facilities. These experiments are in two general classes. In the first class, a shock wave is propagated into a nonflowing (or very slowly flowing) gas ionized by electric discharge.[12] In the second class, a model (usually a small sphere) is projected at supersonic velocities into an ionized, nonflowing gas at a ballistic range.[13] In both classes of experiments, the test duration is of the order of hundreds of microseconds, and the shock structure must be observed on the fly, during a short period as the structure passes the measurement stations.

A second complexity is the control and measurement of the test plasma parameters. It is desirable to have uniform gas temperature (or internal energy distribution), species concentrations, and electron temperature and density throughout the test region, and these should remain constant except as perturbed by the passing shock structure. These are difficult test conditions to achieve in electric discharges in gases. Such conditions are more easily achievable in thermal plasmas, in which the test gas is heated to a uniformly high temperature and the ionization level is determined by the Saha equilibrium. However, all of the experiments for which shock weakening is reported occur in a nonequilibrium plasma, for which the ionization level is considerably above that provided by equilibrium ionization. It is difficult to guarantee uniform properties in such plasmas,

Received 31 August 1999; revision received 17 January 2000; accepted for publication 9 February 2000.

*Graduate Research Assistant, Nonequilibrium Thermodynamics Laboratory, Department of Mechanical Engineering.

†Postdoctoral Researcher, Nonequilibrium Thermodynamics Laboratory, Department of Mechanical Engineering.

‡Undergraduate Research Assistant, Nonequilibrium Thermodynamics Laboratory, Department of Mechanical Engineering.

§Research Scientist, Nonequilibrium Thermodynamics Laboratory, Department of Mechanical Engineering. Senior Member AIAA.

¶Associate Professor, Nonequilibrium Thermodynamics Laboratory, Department of Mechanical Engineering. Senior Member AIAA.

**Professor, Nonequilibrium Thermodynamics Laboratory, Department of Mechanical Engineering. Senior Member AIAA.

††Ralph W. Kurtz Professor, Nonequilibrium Thermodynamics Laboratory, Department of Mechanical Engineering. Associate Fellow AIAA.

and in the absence of equilibrium, it also becomes mandatory to investigate the internal mode energy distribution. Improved control and measurement of plasma properties in the test gas is needed.

The experiments reported here represent an effort to address and circumvent the complexities noted in previous experiments. The present experiments are conducted in a new, unique, steady-state supersonic flow facility, with well-characterized, near uniform, nonequilibrium plasma properties.

II. Experimental Facility

The present experiments are conducted in a new, small-scale, nonequilibrium plasma wind tunnel recently developed at Ohio State University (OSU). It provides a steady-state supersonic flow of cold nonequilibrium plasma with well-characterized, near uniform, properties. The steady-state operation is an obvious advantage compared with short runtime supersonic flow studies in shock tubes and ballistic ranges. The wind tunnel is the high-pressure-discharge/supersonic-flowing-afterglow apparatus shown in Fig. 1. The flow direction is indicated by the arrows.

The upstream discharge section, labeled in Fig. 1, is a contoured quartz tube of rectangular cross section, with dimensions of 6 by 10 mm at the upstream end and 3.5 by 6.5 mm at the smaller end attached to a throat of the supersonic nozzle. The throat is made of a $\frac{1}{8}$-in. copper flange, which forms the downstream electrode of the discharge. The effective length, from the upstream injector/anode end to the downstream nozzle-throat/cathode end, is $L = 4$ cm. The discharge is powered by a regulated, current-limited, 50 kV/50 mA dc power supply (Del Corporation Model RHVS 50-2500). The discharge power circuit is ballasted by 400 kΩ resistance in series with the discharge load. Details of the design and operational characteristics of aerodynamically stabilized glow discharge sustained in tubes of this type, previously used in N_2/CO_2 and CO gas lasers, are given in Refs. 20–22. Basically, the aerodynamic stabilization technique involves injecting the entire gas flow into the discharge through small slots on the top and bottom walls of the discharge tube, as shown in Fig. 1. Small copper strips flush with the slot edges form the anode. Flow through the slots is choked, so that gas velocity past the anode is sonic, and gas density is relatively high. Immediately after the slot, the gases expand (subsonically) into the discharge tube and flow through the discharge at lower velocities. This design insures a high-speed, relatively dense, gas flow across the face of the anode. This flow is transverse to the current direction. Incipient arc filaments, that is, regions of higher temperature and lower density, which could coalesce into arc breakdown, are convectively dissipated by this fast transverse flow. This technique, combined with current limiters in the power supply, inhibits arc formation and subsequent glow-to-arc contraction in the discharge. It becomes possible to run a diffuse glow discharge at very high pressures. Typically, a conventional glow discharge collapses into an arc at pressures of a few tens of torr (Ref. 23). The present device maintains a true glow at pressures of at least $\frac{2}{3}$ atm in pure molecular gases (such as N_2), and of at least 6 atm in mixtures of these gases with He, which improves thermal transport in the positive column.[20–22] In the present experiments, discharge pressure was varied from $\frac{1}{3}$ to 1.5 atm. With pure N_2 in the tube, at the pressure of $\frac{2}{3}$ atm, the applied voltage is $U = 34$ kV at the discharge current of $I = 20$ mA, and the input power to the discharge is 680 W, which gives a power loading into the discharge tube of ~ 400 W/cm^3. At these conditions, the entire discharge section is filled with the positive column of the glow with uniform emission intensity. If current is increased beyond the 20-mA level, incipient arc filaments are observed, forming and extinguishing. Further current increase results in contraction of the discharge into a single, narrow, very bright arc. The device is not generally run to this limit because the action of the arc, specifically the gas heating and the rapid erosion of the electrodes, can cause severe damage.

The physics and kinetics of such a glow, in particular strongly different temperatures of electrons and the heavy species, as well as the extreme nonequilibrium distribution of energy among the vibrational and translational modes of molecules in molecular gases, are well known and understood.[23,24] Figures 2 and 3 shows electron energy balance and electron temperature in glow discharges in N_2 and in He, calculated as a function of the reduced electric field, that is, the ratio of the electric field to the total number density, E/N (Refs. 25 and 26). One can see that for the experimental conditions in pure N_2, described in the preceding paragraph, $E/N \cong U/LN = 5 \times 10^{-16}$ V cm^2, electron temperature is $T_e = 1.5$ eV, and about 95% of the input electrical power is going

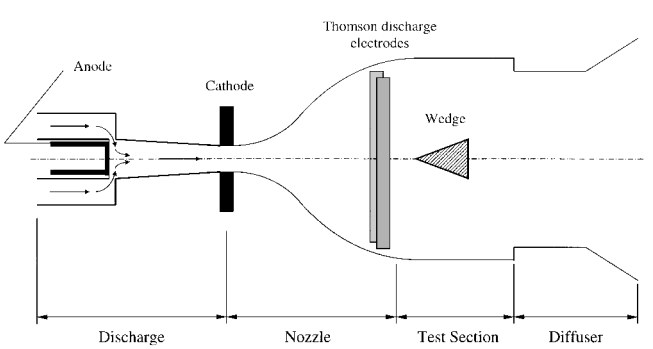

Fig. 1 Schematic of wind-tunnel experiment.

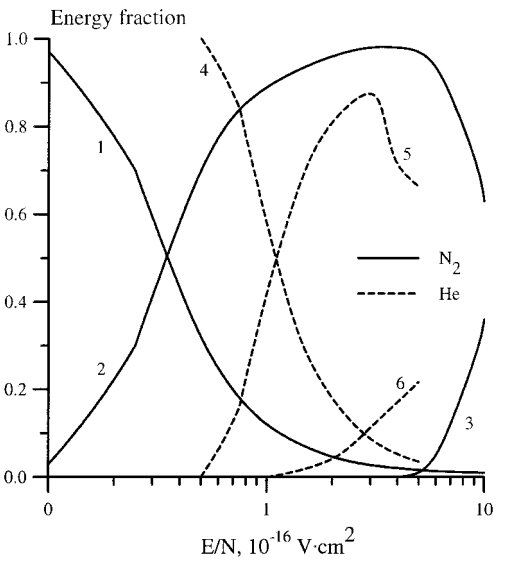

Fig. 2 Electron energy balance in N_2 and He plasmas; ——, N_2: 1) elastic collisions, 2) vibrational excitation, and 3) electronic excitation; and – – –, He: 4) elastic collisions, 5) electronic excitation, and 6) ionization.

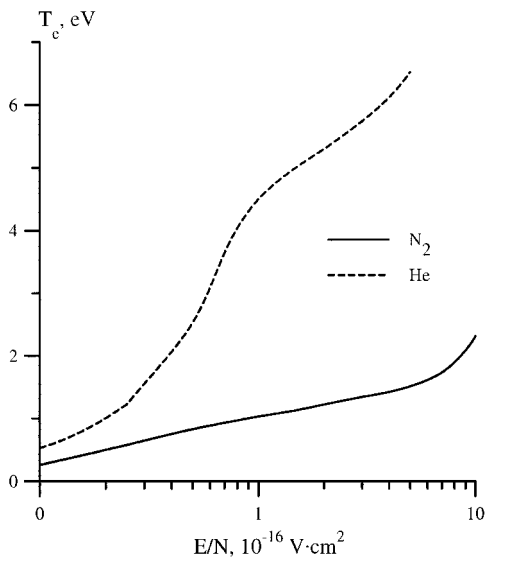

Fig. 3 Electron temperature in N_2 and He plasmas.

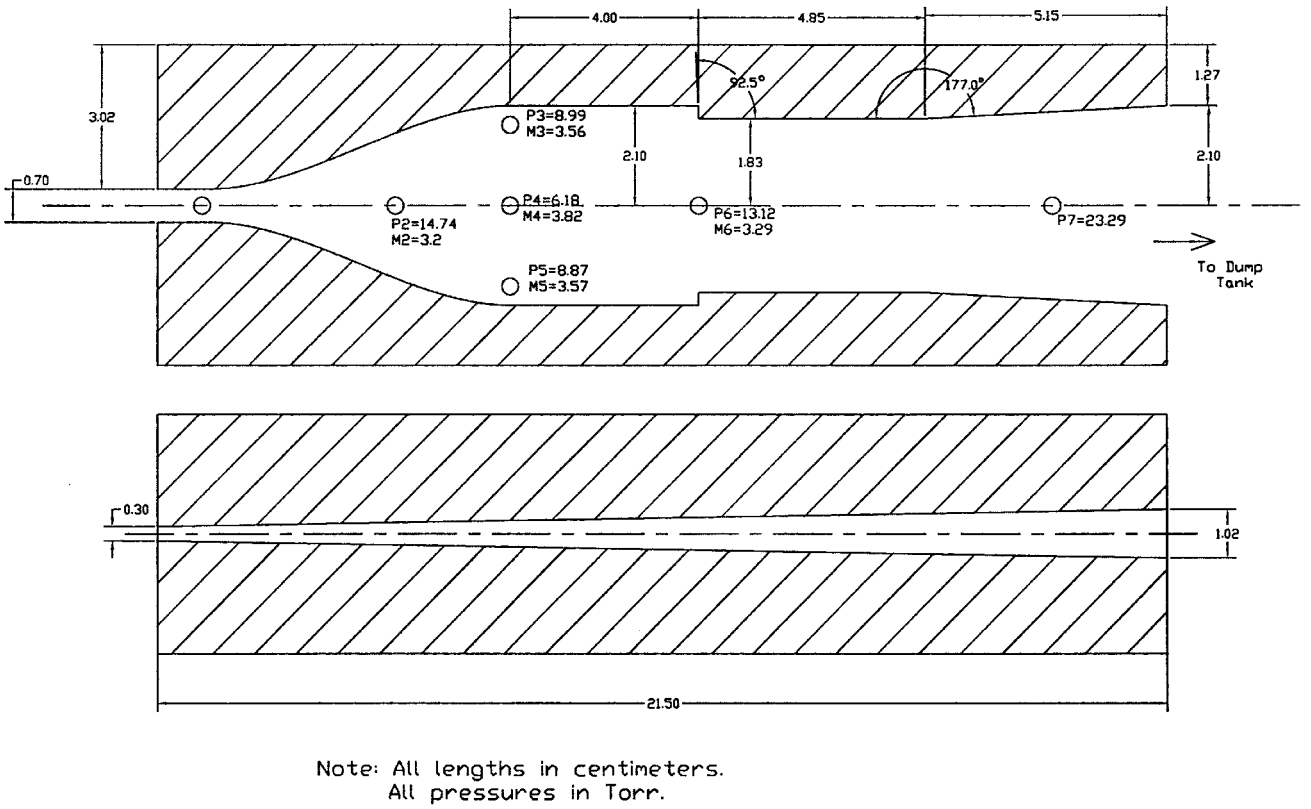

Fig. 4 Supersonic nozzle with pressure taps; static pressures are measured in a nitrogen flow at $P_0 = 1$ atm.

into the vibrational mode of N_2. This gives the vibrational temperature of N_2 $T_v \cong \omega_e / \ell n(\omega_e RG/UI) = 2000$ K. Here $\omega_e = 3395$ K is the vibrational quantum of N_2, and $G = 3.5$ g/s is the mass flow rate. In contrast to an electric arc, very little power goes directly to gas heating. The translational temperature rise in the discharge is $\Delta T = 0.05 \cdot UI/c_p G \cong 10$ K. Note that complete vibrational relaxation of nitrogen would result in a much higher temperature rise, $\Delta T \cong 200$ K.

In helium at $\frac{2}{3}$ atm, the discharge voltage is much lower, $U =$ 7.4 kV at $I = 10$ mA ($E/N = 1.1 \times 10^{-16}$ V cm^2, $T_e = 4.5$ eV). The electron temperature in He plasma is higher, even though the electric field is lower, because the electrons do not lose their energy to vibrational excitation, as occurs in N_2. At these conditions, a much greater power fraction, about 60%, goes to direct heating, the rest being contributed into excitation of the metastable levels, He(2^1S,2^3S) (see Fig. 2). However, even if all discharge power in He is instantaneously converted into heat, the temperature will also rise by only $\Delta T \cong 10$ K (the mass flow rate of helium at these conditions is $G = 1.4$ g/s). The average electron density, inferred from the measured discharge voltage, current, and pressure, is $n_e = 2 \times 10^{10}$ cm^{-3} in N_2 and $n_e = 3 \times 10^{10}$ cm^{-3} in He, and the ionization fractions are $n_e/N = 10^{-9}$ and 1.5×10^{-9}, respectively. This electron density is typical for glow discharges; the rather low ionization fraction reflects the unusually high operating pressure of the electric discharge. These calculations show that conditions of the gases at the throat exhibit the marked thermal disequilibrium characteristic of the positive column of a glow discharge.

Static pressure upstream of the throat is measured using wall taps connected to capacitance manometers (MKS Baratron), in the following locations: 1) in the delivery line to the discharge, upstream of the gas injector for the discharge, and 2) in the discharge section. For optimum operation of the aerodynamically stabilized discharge, the flow through the injector, into the discharge, should be choked. For this, the pressure upstream of the injector should be approximately double the discharge pressure. Both pressures were measured for all runs.

Downstream of the discharge section that forms the high-pressure plenum is the two-dimensional supersonic nozzle of rectangular cross section, shown in Figs. 1 and 4. The top and bottom surfaces of the channel slightly diverge to allow for boundary-layer displacement, as shown on the side view in Fig. 4. The nozzle is made of transparent acrylic plastic, which allows optical access to the expansion. The nozzle is aerodynamically contoured to provide boundary-layer relief and uniform supersonic flow in the test section at a Mach number in the $M = 3$ range. Fabrication and use of a range of nozzles with varying expansion ratios and test section lengths is straightforward and rapid. The system is connected, through a simple channel diffuser, to a ballast tank pumped by a several-hundred-cubic-feet-per-minute vacuum pump.

Static pressure measurements in the supersonic flow are performed using a separate nozzle equipped with the pressure taps shown in Fig. 4. Pressure is measured at three axial locations along the nozzle expansion, in the test section, and at the entrance to the diffuser. In addition to all of these axial measurements, at the end of the nozzle, two additional taps measured the transverse pressure distribution, as shown in Fig. 4.

A 30-deg total angle, 2-cm-long wedge is inserted into the supersonic ionized flow in the nozzle as shown in Fig. 1. The wedge leading-edge diameter is less than $\frac{1}{2}$ mm. The wedge is intended for the study of possible dispersion/weakening of the oblique shock attached to the wedge in the nonequilibrium plasma flow. The wedge extends from the top to the bottom wall of the flow channel, that is, this reasonably approximates a two-dimension flow. The leading edge of the wedge is 0.3 cm downstream of the end of the nozzle section, that is, 0.3 cm downstream of position 4 in Fig. 4. The wedge extends for 2 cm in the downstream direction, forming an isosceles triangular planform with apex pointing upstream.

The test section Reynolds number is in the range $Re_x = (3\text{–}5) \times 10^5$, which is in the boundary-layer transition region.[27] However, a strong negative pressure gradient existing in the nozzle, which is known to be a stabilizing factor, might significantly delay the transition point in the boundary layer on the nozzle walls.[27] Note that for the boundary layer growing on the wedge the Reynolds number is lower by about an order of magnitude, so that it is most likely to be laminar.

Summarizing, the system is, in effect, a small supersonic plasma wind tunnel, but with a critical difference: This is not an arc-heated

tunnel. The electric discharge is a diffuse glow achieving a nonequilibrium gas state in the tunnel plenum. This state is characterized by high vibrational temperature in molecular gases (~2000 K), high electron temperature (a few electron volts), and a low rotational/translational mode temperature (~300 K). The aerodynamic stabilization technique employed inhibits glow-to-arc transition in the discharge, and permits stable glow discharge operation at nearly atmospheric pressures. Operation at such relatively high plenum pressures creates a supersonic flow of reasonable quality in the test section of the tunnel. As we will show, the flow in the test section is typically ~80% inviscid core (see Sec. III.A).

III. Results and Discussion

A. Gasdynamic Performance

Extensive gasdynamic tests were conducted to determine the extent and duration of the supersonic test flows that could be achieved in the tunnel shown in Fig. 4. In these tests, the tunnel was operated with dry air or nitrogen, expanded from $P_0 = 1$ atm plenum conditions, with the electric discharge turned off. The static pressures P_i (torr) measured during such a test are recorded in Fig. 4, next to the correspondingly numbered measurement tap. Shown immediately below the pressure reading is the effective Mach number of the flow at that tap location, inferred from the measured pressure ratio P_0/P_i and the standard isentropic relation, $P_0/P_i = [1 + (\gamma - 1)M^2/2]^{\gamma/(\gamma-1)}$. It can be seen that the flow accelerates to $M = 3.8$ at the entrance to the test section. The flow is supersonic, and the Mach number is reasonably constant across most of the channel at this location. As indicated by the transverse pressure readings at taps 3 and 5, the flow is slightly slower nearer the walls, at the beginning of the boundary layer. At the diffuser entrance, there is already a shock pattern decelerating the flow, and the pressure begins to rise (tap 6). The most downstream measurement, at tap 7, near the diffuser outlet, gives an indication of a very moderate recovery afforded by the simple diffuser geometry for such a relatively low-density expansion. The pressure at the diffuser exit is $P_7 = 23.3$ torr, giving a recovery factor of only $P_7/P_0 = 0.03$. When the pressure in the dump tank, downstream of the diffuser, is allowed to rise to values exceeding P_7, a shock pattern moves up the diffuser into the test section, eventually ending the supersonic flow. Static pressure at the entrance to the test section, P_4, has also been measured as a function of time during a run when the ballast tank pump was valved off and the back pressure allowed to rise as the tank filled. This showed that a steady, $M = 3.8$ supersonic flow corresponding to $P_4 = 6.2$ torr is maintained for about 60 s. Pressure measurements with the pump turned on demonstrated that the supersonic flow can be sustained indefinitely long.

The planar (two-dimensional) nozzle expansion contours were designed for $M = 3$ supersonic operation in the test section. The tests reviewed earlier, showing an $M = 3.8$ test section Mach number, indicate that the divergence of the top and bottom sections (Fig. 4) is an over-correction for boundary-layer growth. The higher-than-design Mach number is created by some expansion of the core flow in the vertical direction. Accordingly, all subsequent tests in the program were conducted with the nozzle top and bottom divergence slightly modified from that shown in Fig. 4. In all subsequent tests, dimensions and contour are the same as shown in Fig. 4, with the single exception that the height of the channel at the diffuser exit was 0.65 cm, rather than the 1.02 cm value shown. With this modification, static pressure at the test section corresponded to $M = 3$ operation; overall operation and relative pressure distribution was otherwise similar to that observed earlier.

Measurements of gasdynamic performance of the tunnel with the discharge turned off were compared with results of modeling calculations for a nitrogen flow, performed using the OSU compressible two-dimensional Navier–Stokes code. The code uses the linearized block implicit (LBI) method developed by Briley and McDonald to solve the governing equations.[28] This method was originally developed for the solution of the compressible Navier–Stokes equations for nonreacting flows, with some limited extension to reacting flows.[29] The LBI method has been recently used to solve problems requiring full coupling of state-specific vibrational kinetics with the flow and found to be fast and efficient.[30,31] The calculations have been made for nitrogen flow in a nozzle without the model, for stagnation parameters $P_0 = 1$ atm and $T_0 = 300$ K. The nozzle contour and dimensions used in the calculations are those of Fig. 4. In these calculations, a nonstaggered grid, uniform both in the axial and in the radial directions has been used, with 50 points in the axial direction and 270 points in the radial direction. Figure 5 shows the Mach number contour plot in the nozzle. One can see that the flow in the test section reaches $M = 3$ and that about 80% of the flow is the inviscid core where the Mach number is nearly constant. This is in quite reasonable agreement with the transverse pressure measurements made in the tunnel.

B. Electron Density Measurements

For the measurement of electron density in the supersonic afterglow, the nozzle is equipped with pairs of transverse strip electrodes, placed flush in the top and bottom nozzle walls (Fig. 1). These electrodes are in effect probes, which can be used to infer the electron density in non-self-sustained discharges, such as the present flowing afterglow. The theory of such probes (Thomson discharges; see Ref. 32) is given in our previous paper,[33] where their use for associative ionization studies was reported. Using this technique, the electrons can be almost completely removed from the flow by applied small dc potential across the electrodes. As shown in Ref. 33, the electron concentration can be inferred from the measured saturation current and voltage.

Figure 6 shows a typical voltage–current characteristic from a probe located at the $M = 3$ station at the beginning of the test section. In this test, plenum pressure was $\frac{2}{3}$ atm of N_2. Note that nonzero current (3.7 μA) is drawn at zero applied voltage, which indicates unequal probe electrode potentials. However, the measured potential difference between the test section electrodes turns out to be very weak, about 0.3 V. This weak electric field might be present

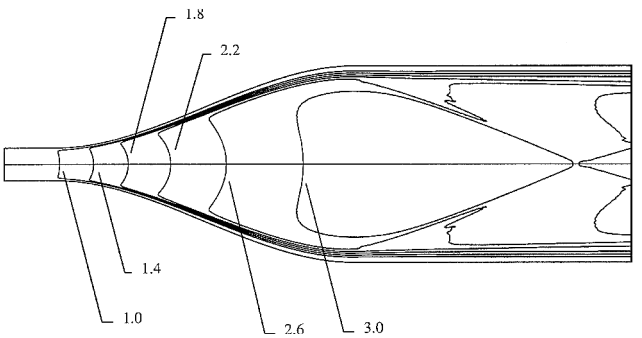

Fig. 5 Mach number contours in the nozzle without the model; nitrogen, $P_0 = 1$ atm, $T_0 = 300$ K.

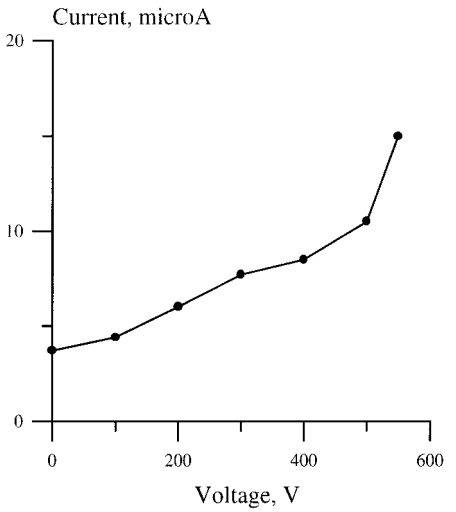

Fig. 6 Current–voltage characteristic of the Thomson discharge in the test section; N_2, $P_0 = \frac{2}{3}$ atm.

in the test section both because the ionized flow is not entirely symmetric and because of the residual electric field created by the electrodes upstream. The probe current increases with increasing bias and nearly saturates at $U = 400$ V. Further current rise, including a sharp increase at $U > 600$ V is due to additional electron impact ionization produced between the transverse electrodes (self-sustained discharge initiation) and breakdown. One can see that the saturation voltage, $U \sim 400$ V, is below breakdown for the gas density $N = 1.2 \times 10^{18}$ cm^{-3} and electrode separation $L = 0.5$ cm, at this point ($E/N \sim U/LN = 6.4 \times 10^{-16}$ V · cm^2). When the plenum discharge in turned off, no current is drawn through the probe at this voltage nor at any lower bias. Therefore, in the saturation region, almost the entire electron flux entering the test section with the gas flow is removed by the applied field, which does not produce any additional ionization. Then the ionization fraction can be found as

$$n_e/N = I_s \mu / eGN_A = 0.7 \times 10^{-9} \quad (1)$$

where $I_s = 8$ μA is the saturation current, $\mu = 28$ is the molecular weight of nitrogen, and $G = 3.5$ g/s is the mass flow rate. Note that it is about the same as in the main discharge, which shows that electron density in the supersonic afterglow decreases roughly proportionally to the total number density, while recombination remains insignificant. Indeed, the flow residence time in the nozzle is about 100 μs, whereas the characteristic recombination time is much longer, $\tau_{\text{rec}} \sim 1/\beta n_e \sim 1$ ms. Here $\beta \sim 10^{-7}$ cm^3/s is the dissociative recombination rate coefficient, and $n_e \sim 10^{10}$ cm^{-3} is the electron density in the plenum. From the known test section number density, $N = 1.2 \times 10^{18}$ cm^{-3} (at $M = 3$, $P = 14$ torr, and $T = 110$ K), electron density in the test section is $n_e = 0.8 \times 10^9$ cm^{-3}.

To draw current between the probe electrodes without the flow between them preionized by the upstream plenum discharge, higher voltages must be applied, creating breakdown. If this is done, the resultant transverse discharge is very inhomogeneous and unstable, primarily producing local arcs through the boundary layer. However, if the probe voltage is increased beyond the near-saturation region, with the plenum discharge on, a different behavior is observed. Figure 7 shows the extended current voltage characteristic, with the applied voltage extending to 1000 V ($E/N \sim 1.6 \times 10^{-15}$ V · cm^2). In the region between 400 and 600 V, a quite uniform transverse discharge across an $M = 3$ flow channel is sustained. Visual observation shows an increasing local luminosity between the probe electrodes, evenly distributed across the inviscid core flow in the channel, but not extending into the boundary-layer regions near the walls. This luminosity increases with the current. Above 600 V, transverse arc filaments begin to appear, and the current abruptly increases from 10 to 100 μA (Fig. 7). Note that in the present study the use of the transverse Thomson discharge[32] is limited only to electron density measurements substantially below the breakdown point.

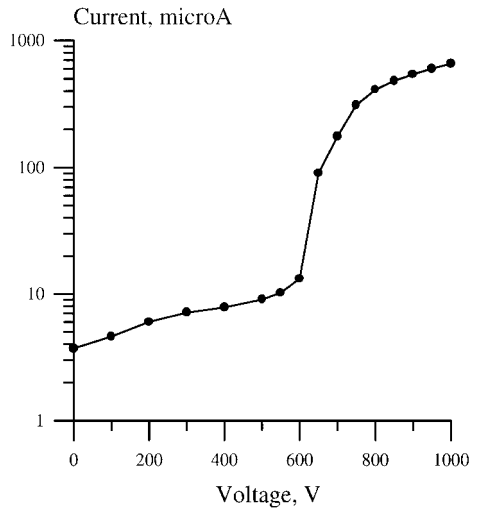

Fig. 7 Extended current–voltage characteristic of the Thomson discharge in the test section; N_2, $P_0 = \frac{2}{3}$ atm.

C. Shock Angle Measurements

A conventional schlieren system was used to visualize the oblique shocks attached to the nose of the wedge model. A schematic of the system is shown in Fig. 8. Shock pictures are recorded with a framing camera, as shown on the schematic. With this system, quite good shock visualization is obtained for runs in air or nitrogen with plenum pressures in the range $0.6 < P_0 < 1.0$ atm. Figure 9 shows a typical schlieren picture of the shock attached to a 30-deg total angle wedge in the tunnel operating at $M = 3.0$ and $P_0 = \frac{2}{3}$ atm of pure N_2. The wedge planform and the quite straight oblique shock on either side of the nose can be seen. The total shock angle, of approximately 65 deg, implies a flow Mach number of 3.1, which is consistent with the measured pressure ratio at the test station.

With this model, and for these flow conditions, an extensive series of test runs were performed to investigate the possible weakening or dispersion of the shock by the effect of ionization in the test flow. The test procedure for these runs was to initiate the flow in the tunnel, to confirm steady-state conditions by static pressure measurements, and to record the shock schlieren picture over several seconds and several frames, with the electric discharge in the plenum off. After this, at several seconds into the run, the plenum electric discharge was struck, with voltage and current set to preselected values. The tunnel operation was continued for several more seconds, and the shock schlieren pictures were again recorded for several frames. Finally, in the same run, the discharge was turned off, and the shock schlieren pictures again were recorded for several frames. During the entire run, the pressures were monitored to ensure that steady supersonic flow was being maintained throughout the test duration and

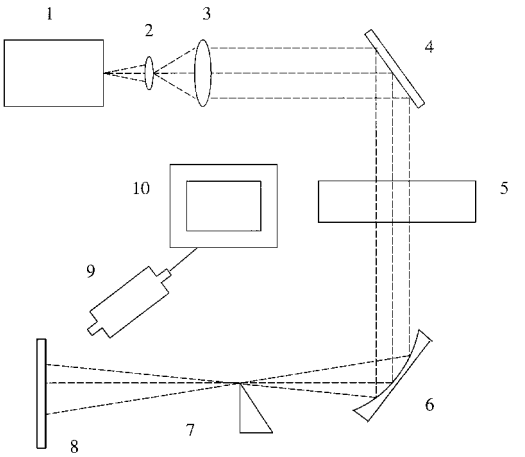

Fig. 8 Schlieren system schematic: 1, 1-kW lamp; 2, iris; 3, lens; 4, plane mirror; 5, nozzle test section; 6, collimating mirror; 7, knife edge; 8, screen; 9, video camera and frame grabber; and 10, personal computer.

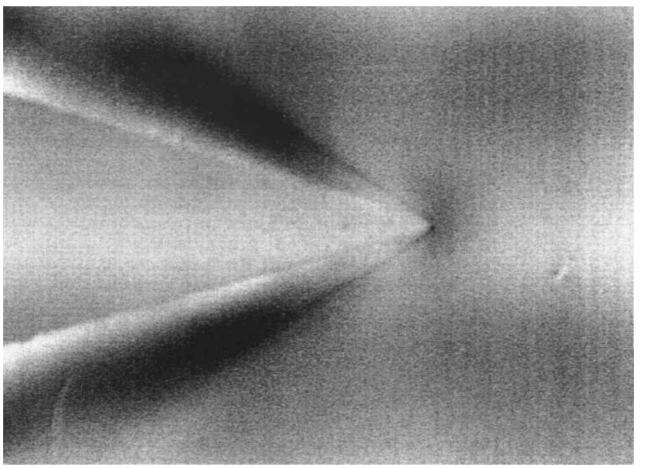

Fig. 9 Typical schlieren image of oblique shocks.

Table 1 Plasma shock angle measurements

Discharge conditions	Flow conditions	Shock angle, deg	Mach number	T/T_0
		Trial 1		
Plasma current: 15.7 mA	Plasma off	$64.65^{+2.02}_{-2.70}$	2.99	0.3588
Plasma power: 529.4 W	Plasma on	$67.43^{+2.82}_{-2.75}$	2.82	0.3866
Pressure: 0.667 Atm N2	Plasma off	$65.55^{+2.35}_{-2.49}$	2.93	0.3681
		Trial 2		
Plasma current: 15.7 mA	Plasma off	$62.99^{+2.44}_{-2.52}$	3.11	0.3414
Plasma power: 529.4 W	Plasma on	$67.77^{+4.88}_{-4.03}$	2.80	0.3899
Pressure: 0.667 Atm N2	Plasma off	$63.94^{+2.63}_{-3.57}$	3.04	0.3515
		Trial 3		
Plasma current: 20.0 mA	Plasma Off	$62.91^{+1.38}_{-1.67}$	3.11	0.3406
Plasma power: 680.0 W	Plasma on	$67.91^{+2.04}_{-1.18}$	2.79	0.3913
Pressure: 0.667 Atm N2	Plasma off	$65.23^{+2.35}_{-2.49}$	2.95	0.3648
		Trial 4		
Plasma current: 20.0 mA	Plasma off	$65.33^{+3.29}_{-3.72}$	2.94	0.3658
Plasma power: 680.0 W	Plasma on	$66.03^{+2.61}_{-3.15}$	2.90	0.3729
Pressure: 0.667 Atm N2	Plasma off	$64.81^{+1.91}_{-2.75}$	2.98	0.3605

that back pressure did not exceed recovery values. Basically, then, a test run consisted of several measurements of shock position for a plasma-off flow, followed by several measurements with plasma on, followed by several more measurements with, again, plasma off.

No substantial breakup or dispersion of the oblique shock was observed in any runs. To determine whether there was any overall change in the shock strength between plasma-on and plasma-off conditions, the shock angle was measured for every frame in each test run. Measurement was by the operator placing cursor lines along the shock front on the computerized schlieren picture and recording the angle as given from the computer. Table 1 is a summary of the data for four such test runs, two for plenum electric discharge currents of 15.7 mA and two for higher input powers, with plenum electric discharge currents of 20 mA. Each of the shock angle measurements reported in Table 1 represent an average of many data frames. It can be seen that the accuracy with which the shock angle can be measured for these conditions is ±3 deg, with the average shock angle being near 66 deg. In addition to the average shock angle measured in the runs, Table 1 also records the Mach number and the temperature ratio T/T_0 corresponding to the measured shock angle. Static pressure at the entrance to the test section was measured during all of these runs. For these, $P = 11.0$ torr, giving $P/P_0 = 0.022$, implying a test section Mach number $M = 3.1$, in excellent agreement with the shock angle measurement, as noted earlier.

With the strongly nonequilibrium nature of the flow, there is no single static temperature characterizing the local (static) flow enthalpy. However, in these continuum flows, the translational and rotational molecular modes are equilibrated, and there is a unique temperature characterizing the energy in these modes. This translational/rotational temperature is what is denoted without further qualification as gas temperature or static temperature T throughout this paper. Stagnation temperature T_0 is defined conventionally: It represents the total temperature that the flow gases would achieve if the gas were to be decelerated to zero velocity and all modes, translation, rotation, vibration, and electronic, were to be brought into thermal equilibrium. Because the total energy input from the discharge into the flow gases is measured, as are the flow velocities, the total (stagnation) flow enthalpy is known, and T_0 is unambiguously inferred. For the higher discharge power loading runs of Table 1, where 680 W were added to the flow, $T_0 = 500$ K.

The static temperature has not been directly measured in the experiments to date. However, the energy distribution in the discharge and plenum is well characterized, as discussed in Sec. II. Using the measured flow and plasma data, the nonequilibrium gasdynamic flow modeling code has been run for the test conditions. The details of these calculations are given in the Appendix. As shown there, there is very little loss of energy from the vibrational mode in the supersonic expansion and, therefore, negligible rise in the static temperature due to such internal energy transfer. This effect causes static temperature increase in the test section core flow by less than 5 K, even for the most extreme power loading conditions. As shown in Table 2, the test section static temperature for all of these runs is low, $T = 100$ K.

Table 2 Calculated test section parameters

Discharge power, W	Static temperature	Mach number	Vibrational temperature	Stagnation temperature
0	98	3.24	300	300
120	98	3.24	1000	335
767[a]	99	3.23	2000	522
1628	103	3.21	3000	772

[a]Close to the experimentally measured value of 700 W.

The data of Table 1 do not seem to show a detectable shock movement between the plasma-on and plasma-off conditions. Whereas some of the data seem to show a slight weakening of the shock (larger shock angles) with the plasma on, the change is well within the scatter of the data. More recent runs, with better schlieren imaging than the data used in Table 1, also support this conclusion. No significant shock movement is seen for these run conditions. In addition to the use of operator-positioned cursors to measure the shock angle, plasma-on images have been computer-differenced with the corresponding plasma-off images for the same run. Again, no significant change in shock strength can be detected.

We conclude that for these test conditions, at least, any change in shock angle due to ionization in the flow is less than 3 deg. As shown in Table 1, the corresponding change in the apparent Mach number is less than 0.3, that is, a Mach number change of less than 10% at the $M = 3$ test conditions. Such change is well below the weakening effects reported in some of the literature; however, any greater change would have been readily detectable by the present experiments.

D. Flow Visualization

Further experiments with the electric discharge turned on demonstrated that the use of the schlieren system is not necessary for shock visualization. During these experiments, the nozzle, test section, and diffuser are filled with the bright visible emission, arising primarily from the well-known orange–red first positive bands, $B^3\Pi_g \rightarrow A^3\Sigma_u^+$, in nitrogen (Fig. 10) and from the blue line of helium (Fig. 11). Multiple features observed in the helium spectrum in the region between 400 and 800 nm (Fig. 11) are most likely due to the air impurity in the gas lines.

Figures 12–14 show black and white photographs of the nozzle filled with the nitrogen (Figs. 12 and 13) and the helium (Fig. 14) afterglow plasmas and the model in place. These photographs are taken with a hand-held 35-mm camera. Color photographs of the

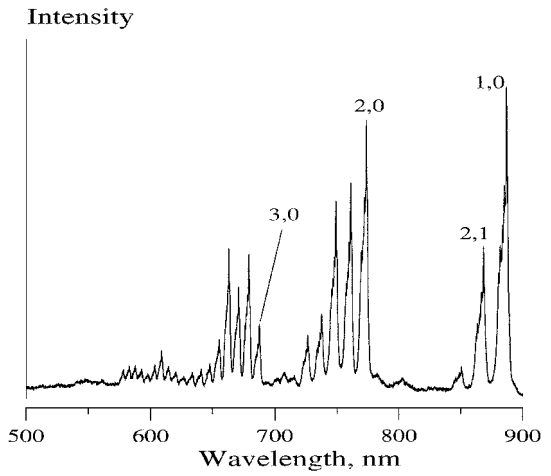

Fig. 10 Visible spectrum of the supersonic flowing afterglow in nitrogen (first positive system bands, $B^3\Pi_g, v' \rightarrow A^3\Sigma_u^+, v''$); values of v' and v'' indicated.

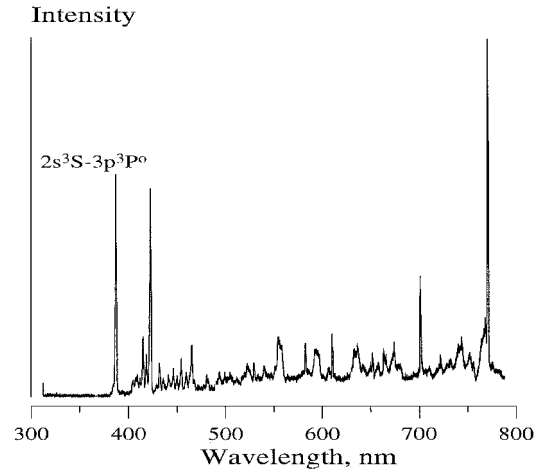

Fig. 11 Visible spectrum of the supersonic flowing afterglow in helium; multiple features in the 400–800-nm region are due to air impurity in the gas lines.

supersonic flowing afterglow, which are an especially effective means of displaying the key features of these nonequilibrium flows, may be found at the OSU Nonequlibrium Thermodynamics Group Web page (http://rclsgi.eng.ohio-stateedu/~ lempert/netl/projects.html) or are available by e-mail on request.

Analysis of these photographs allows identification of many key features of the supersonic nozzle flow. In Fig. 12, taken at plenum pressure of $P_0 = \frac{2}{3}$ atm, a pair of bright hairline oblique shocks attached to the wedge nose are clearly visible. The total shock angle, $\theta = 65$ deg, is in excellent agreement with the schlieren measurements (Fig. 9). Figure 13, taken at the same plenum pressure of $\frac{2}{3}$ atm, shows a somewhat stronger bow shock in front of the blunt body, which is visibly brighter than the shocks in Fig. 12. In addition to the primary oblique shocks, Fig. 12 also displays a pair of fainter secondary oblique shocks produced by the supersonic flow reflection off the luminous boundary layer growing on the wedge walls. Boundary layers in Fig. 12 extend downstream of the wedge as bright shear layers hugging the dark wake. The boundary layer in Fig. 13 separates both from the bow shock and from the model wall upstream of the junction of the half-cylinder and the rectangular section of the model, creating a bright double arch. Luminous boundary layers can be also seen on the nozzle walls (Figs. 12 and 13).

In both Figs. 12 and 13, dark areas where the flow separates from the nozzle and the model walls, as well as dark recirculation regions in the wake of the models, can be noticed. Note that the separation region between the boundary layer and the model wall and the wake behind the model in Fig. 13 have different luminosity and, therefore, can be easily distinguished. Finally, Figs. 12 and 13 demonstrate regular patterns of brighter and darker bands that look somewhat

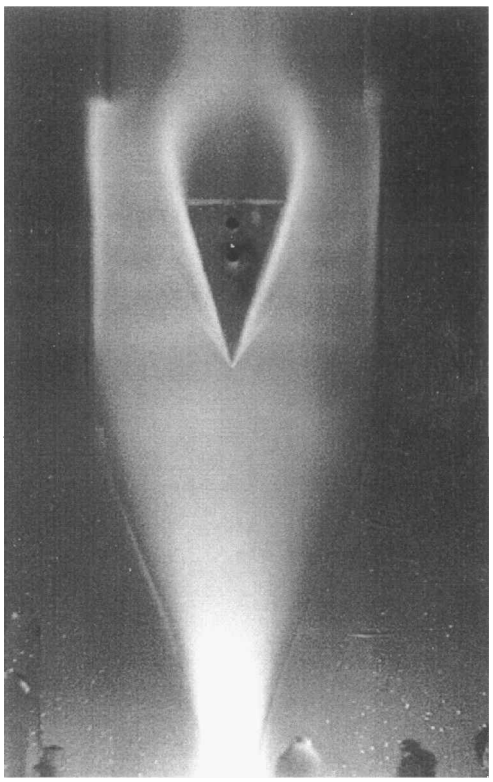

Fig. 12 Photograph of the supersonic nitrogen plasma flow around a wedge; $P_0 = \frac{2}{3}$ atm.

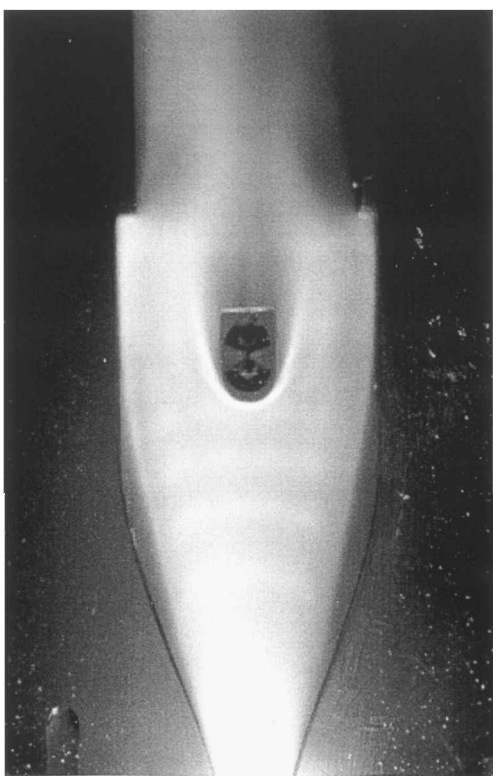

Fig. 13 Photograph of the supersonic nitrogen plasma flow around a blunt body; $P_0 = \frac{2}{3}$ atm.

similar to striations (weak ionization instabilities) frequently observed in glow discharges.[23] In the present experiments, the bands are also observed in supersonic afterglow without the model. Note that this periodic structure appears far downstream of the discharge section where the electric field, which sustains striations in the glow discharge, is very weak (see Sec. III.B). Therefore, we suggest that this intensity alteration indicates the relaxation instability sustained by the energy storage in metastable states of N_2 and He.

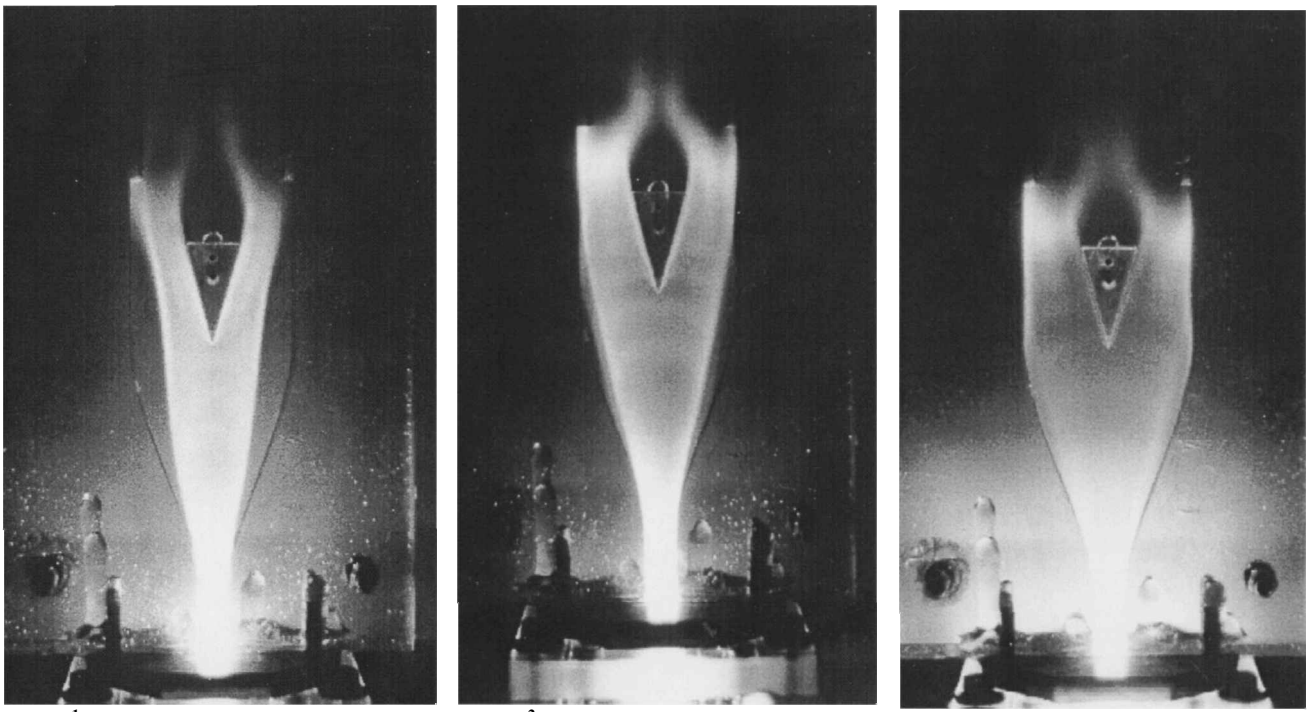

a) $P_0 = \frac{1}{3}$ atm b) $P_0 = \frac{2}{3}$ atm c) $P_0 = 1.5$ atm

Fig. 14 Photographs of the supersonic helium plasma flows around a wedge.

Figure 14 shows photographs of He plasma afterglow for three different plenum pressures of $\frac{1}{3}$, $\frac{2}{3}$, and 1.5 atm. These three photographs display the flow features similar to those observed in the nitrogen afterglow (Fig. 12). The somewhat curved oblique shocks are most clearly visible at the lowest plenum pressure, $P_0 = \frac{1}{3}$ atm (Fig. 14a), when the radiation intensity is also the highest. The dark separation regions are noticeably reduced at higher plenum pressure, $P_0 = \frac{2}{3}$ atm, and almost completely disappear at $P_0 = 1.5$ atm (Figs. 14b and 14c). The luminous boundary layers, the dark wake regions, and the periodic intensity patterns are visible on all three photographs.

All of these spectacular features can be easily observed in real time simply by looking at the wind tunnel during its operation. In particular, these observations show that all flow features, including the periodic intensity patterns, are steady (nonmoving) as long as the flow in the nozzle remains supersonic. The oblique shock pattern, moving upstream into the test section as the dump tank pressure increases and terminating the supersonic flow, is also clearly visible. We conclude that the two-dimensional flowing afterglow technique allows accurate flow visualization, including shocks, boundary layers, wakes, and recirculating flow regions. Although the use of nonequilibrium radiation from the species excited by electron beam or by electric discharge for flow visualization is well known (see Ref. 34 and the references therein), it was previously limited only to the low-density flows ($N \sim 10^{15}$–10^{16} cm^{-3}). The present method, however, allows flow visualization at densities at least up to $N \sim 10^{18}$ cm^{-3}.

Interpretation and quantitative analysis of the observed radiation intensity distribution, as well as establishment of its correlation with the flowfield, require kinetic modeling of nonequilibrium viscous supersonic flows. In some cases the full coupling of kinetics with the flowfield can be replaced by an overlay approach, which assumes that relaxation of energy stored in atomic and molecular metastables has no effect of the flow. This assumption is certainly justified for helium afterglow because the amount of energy stored in helium metastables is negligible compared to the flow enthalpy (see Sec. II). In nitrogen, however, this assumption can be used only for semiqualitative interpretation of the observed flow features because a substantial portion of the flow enthalpy is stored in the vibrational mode (see Sec. II). In the inviscid core flow, the nitrogen vibrational energy is essentially frozen at the throat values (vibrational relaxation time of pure N_2 at room temperature is of the order of a second at atmospheric pressure). However, nitrogen will vibrationally relax in boundary layers, where the flow reaches near stagnation, thereby raising the temperature and affecting the flowfield.

Qualitatively, the intense radiation from the shock regions (Figs. 12–14) is likely to be explained without involving kinetics, simply by the proportional increase of the radiating species densities to the rise of the total number density across the shock. The absence of visible radiation from the flow separation regions and wakes is most likely due to the long flow residence time in these regions, which results in nearly complete relaxation of the excited species. Finally, the interpretation of the high luminosity of the boundary and shear layers (Figs. 12–14) does require analysis of kinetics. In nitrogen, a qualitative scenario might include the following successive stages: 1) nitrogen vibration–vibration (V–V) pumping

$$N_2(X, v) + N_2(X, w) \leftrightarrow N_2(X, v-1) + N_2(X, w+1) \qquad (2)$$

which overpopulates the high vibrational levels of the ground electronic state, $N_2(X^1\Sigma_g^+, v)$ (Ref. 35), 2) increase of the $A^3\Sigma_u^+$ metastable state population due to coupling with the high vibrational levels of the X state[36]

$$N_2(X, v) + N_2(X, w) \leftrightarrow N_2(A) + N_2(X), \qquad E_v + E_w \geq 6.2 \text{ eV} \qquad (3)$$

and 3) population of the $B^3\Pi_g$ and $C^3\Pi_u$ radiating states by rapid energy pooling processes[36]

$$N_2(A) + N_2(A) \rightarrow N_2(B) + N_2(X)$$
$$N_2(C) + N_2(X) \qquad (4)$$

Because V–V pumping in nitrogen is a relatively slow process[37] and occurs predominantly in the regions where the flow residence time is long, this would result in the rise of radiation intensity in the boundary and shear layers. Another process that might produce $N_2(A^3\Sigma_u^+)$ in the boundary layer, nitrogen atom recombination,[38] might also contribute to this effect.

On the other hand, the similarity of the radiation intensity patterns in N_2 and He, in particular the bright boundary layers observed in both gases (Figs. 12–14) suggests a possibility that the increase in the radiating state populations near the wall might be produced by the similar kinetic mechanisms, such as rapid electron–ion recombination on the wall with production of electronically excited

species, and subsequent radiation. Additional diagnostics, such as visible spectra and electron density measurements at several locations in the flow and in the boundary layer may clarify this issue. These measurements are certainly feasible due to long test times available. Also, full coupling of the Navier–Stokes flow code with the state-specific kinetic models, such as been done in Refs. 30 and 31, and incorporation of kinetic processes on the wall is desirable for quantitative analysis of the flowfield.

IV. Summary

The experiments conducted in a new, small-scale, nonequilibrium plasma wind-tunnel facility are described. The facility provides a steady-state quasi-two-dimensional supersonic flow of cold nonequilibrium plasma with well-characterized, near uniform, properties. The available runtime ranges from tens of seconds to a complete steady state. The plasma is produced in aerodynamically stabilized high-pressure glow discharge that forms the plenum of the supersonic nozzle. The possible modification of the supersonic flow due to ionization is studied by measuring the angle of oblique shocks attached to the wedge located in the nozzle test section. The results do not show any detectable shock weakening or attenuation in weakly ionized nitrogen plasma, compared to the measurements in a nonionized gas flow. Additional experiments in ionized flows with higher electron density are suggested.

The experiments in supersonic flowing nitrogen and helium afterglow using this facility demonstrate a novel technique for supersonic flow visualization. It allows identifying all key features of the flow, including shocks, boundary layers, flow separation regions, and wakes by recording intense visible radiation of the weakly ionized plasmas. Interpretation of radiation intensity distributions in nonequilibrium supersonic flowing afterglow may provide information on key mechanisms of energy storage in metastable (dark) states and persistent ultraviolet radiation in high-altitude rocket plumes. In addition, these flow visualization experiments can be used for validation of computer flow codes used for internal flow modeling. Development of the fully coupled nonequlibrium flow code that incorporates key processes of energy storage in meatastable states and nonequilibrium radiation is suggested.

Appendix: One-Dimensional Nonequilibrium Flow Calculations

To estimate the effect of the gas flow heating due to relaxation of energy stored in vibrational degrees of freedom of nitrogen, we used quasi-one-dimensional nonequilibrium flow modeling calculations.[39] The code used solves coupled one-dimensional gas-dynamics equations, master equation for the populations of vibrational levels of molecules, and Boltzmann equation for the electrons. The kinetic model incorporates 1) processes of vibrational excitation of molecules by electron impact in the electric discharge section, 2) vibrational–translational and V–V energy transfer processes that are primarily responsible for the flow heating in the supersonic afterglow, and 3) electron heating in collisions with vibrationally excited molecules (also known as superelastic processes). The objective of these calculations was to determine whether the flow heating by vibrational relaxation is enough to cause substantial changes in the test section Mach number and, therefore, in the oblique shock angle.

The calculations have been performed for nitrogen at stagnation pressure of $P_0 = 500$ torr and stagnation temperature of $T_0 = 300$ K. The nozzle throat cross-sectional area was $A^* = 0.21$ cm^2, with the area ratio $A/A^* = 5.2$, and the length of the supersonic section $L = 10$ cm.

Table 2 shows that for discharge power used in the experiments the flow heating in the inviscid core is negligibly small (static temperature in the test section increases by only about 1–5 K). This occurs due to the slow rate of vibrational energy relaxation in V–V processes and short residence time. However, heating might well be a major factor in the boundary layer where the flow is near stagnation and, therefore, has enough time to vibrationally relax. Indeed, for typical experimental conditions, the stagnation temperature increase due to power loading by the discharge is about 200 K.

In these calculations, the electron temperature in the test section was very close to the vibrational temperature of N_2 (within 50–100 K). This result illustrates a well-known strong coupling between the vibrationally excited molecules and free electrons.[25]

Acknowledgments

This research was supported by the Division of Aerospace and Materials Sciences of the Air Force Office of Scientific Research (AFOSR), and by MSE, Inc., under a NASA prime. The support of the Director of Defense Research and Engineering Air Plasma Ramparts MURI Program, managed by AFOSR for the construction of the supersonic flowing afterglow apparatus is gratefully acknowledged. We wish also to thank Richard Bergman, Jean-Luc Cambier, Harvey Lam, and Sergey Macheret for helpful consultation and advice.

References

[1]Klimov, A. I., Koblov, A. N., Mishin, G. I., Serov, Y. L., and Yavor, I. P., "Shock Wave Propagation in a Glow Discharge," *Soviet Physics—Technical Physics Letters*, Vol. 8, No. 4, 1982, pp. 192–194.

[2]Klimov, A. I., Koblov, A. N., Mishin, G. I., Serov, Y. L., Khodataev, K. V., and Yavor, I. P., "Shock Wave Propagation in a Decaying Plasma," *Soviet Physics—Technical Physics Letters*, Vol. 8, No. 5, 1982, pp. 240, 241.

[3]Basargin, I. V., and Mishin, G. I., "Probe Studies of Shock Waves in the Plasma of a Transverse Glow Discharge," *Soviet Physics—Technical Physics Letters*, Vol. 11, No. 11, 1985, pp. 535–538.

[4]Gorshkov, V. A., Klimov, A. I., Mishin, G. I., Fedotov, A. B., and Yavor, I. P., "Behavior of Electron Density in a Weakly Ionized Nonequilibrium Plasma with a Propagating Shock Wave," *Soviet Physics—Technical Physics*, Vol. 32, No. 10, 1987, pp. 1138–1141.

[5]Ershov, A. P., Klishin, S. V., Kuzovnikov, A. A., Ponomareva, S. E., and Pyt'ev, Y. P., "Application of the Reduction Method to the Microwave Interferometry of Shock Waves in Weakly Ionized Plasma," *Soviet Physics—Technical Physics*, Vol. 34, No. 8, 1989, pp. 936, 937.

[6]Basargin, I. V., and Mishin, G. I., "Precursor of Shock Wave in Glow-Discharge Plasma," *Soviet Physics—Technical Physics Letters*, Vol. 15, No. 4, 1989, pp. 311–313.

[7]Bystrov, S. A., Zaslonko, I. S., Mukoseev, Y. K., and Shugaev, F. V., "Precursor Ahead of a Shock Front in an RF Discharge Plasma," *Soviet Physics—Doklady*, Vol. 35, No. 1, 1990, pp. 39, 40.

[8]Mishin, G. I., Serov, Y. L., and Yavor, I. P., "Flow Around a Sphere Moving Supersonically in a Gas-Discharge Plasma," *Soviet Physics—Technical Physics Letters*, Vol. 17, No. 6, 1991, pp. 413–416.

[9]Mishin, G. I., Klimov, A. I., and Gridin, A. Y., "Measurements of the Pressure and Density in Shock Waves in a Gas Discharge Plasma," *Soviet Physics—Technical Physics Letters*, Vol. 17, No. 8, 1992, pp. 602–604.

[10]Gridin, A. Y., Klimov, A. I., and Khodataev, K. V., "Propagation of Shock Waves in a Nonuniform Transverse Pulsed Discharge," *High Temperature*, Vol. 32, No. 4, 1994, pp. 454–457.

[11]Bedin, A. P., and Mishin, G. I., "Ballistic Studies of the Aerodynamic Drag on a Sphere in Ionized Air," *Technical Physics Letters*, Vol. 21, No. 1, 1995, pp. 5–7.

[12]Ganguly, B. N., and Bletzinger, P., "Shock Wave Dispersion in Nonequilibrium Plasmas," AIAA Paper 96-4607, Nov. 1996.

[13]Lowry, H. S., Crosswy, C., Sherrouse, L., Smith, P., Price, M., Ruyten, L., and Felderman, J., "Shock Structure of a Spherical Projectile in Weakly Ionized Air," AIAA Paper 99-0600, Jan. 1999.

[14]Vstovskii, G. V., and Kozlov, G. I., "Propagation of Weak Shock Waves in a Vibrationally Excited Gas," *Soviet Physics–Technical Physics*, Vol. 31, No. 8, 1986, pp. 911–914.

[15]Mnatsakanyan, A. K., Naidis, G. V., and Rumyantsev, S. V., "Shock Wave Propagation Through Nonuniform and Nonequilibrium Gas Regions," *Shock Waves and Tubes*, edited by H. Gronig, VCH, Weinheim, Germany, 1988, pp. 201–205.

[16]Bystrov, S. A., Ivanov, V. I., and Shugaev, F. V., "Propagation of Plane Shock Wave in Weakly Ionized Plasma," *Soviet Journal of Plasma Physics*, Vol. 15, No. 5, 1989, pp. 324–326.

[17]Gridin, A. Y., Klimov, A. I., Khodataev, K. V., Shcherbak, N. B., and Shcherbak, S. B., "Two-Dimensional Simulation of Shock Wave Propagation in a Transverse Pulse Glow Discharge with a Heated Cathode Layer," *High Temperature*, Vol. 32, No. 6, 1994, pp. 755–758.

[18]Adamovich, I. V., Subramaniam, V. V., Rich, J. W., and Macheret, S. O., "Shock Wave Propagation in Weakly Ionized Plasmas," AIAA Paper 97-2499, June 1997.

[19]Adamovich, I. V., Subramaniam, V. V., Rich, J. W., and Macheret, S. O., "Phenomenological Analysis of Shock Wave Propagation in Weakly Ionized Plasmas," *AIAA Journal*, Vol. 36, No. 5, 1998, pp. 816–822.

[20]Rich, W., Bergman, R. C., and Lordi, J. A., "Electrically Excited Supersonic Flow Carbon Monoxide Laser," *AIAA Journal*, Vol. 13, No. 1, 1975, pp. 95–101.

[21]Rich, W., Bergman, R. C., and Lordi, J. A., "Carbon Monoxide Laser Systems," Calspan—Univ. of Buffalo Research Center, TR AFAL-TR-78-37, Buffalo, NY, April 1978.

[22]Bergman, R. C., "Gaseous Discharge Stabilized Apparatus and Method," U.S. Patent 4,132,961, Jan. 2, 1979.

[23]Raizer, Y. P., *Gas Discharge Physics*, Springer-Verlag, Berlin, 1991, Chaps. 8 and 9.

[24]Gordiets, B. F., Osipov, V. A., and Shelepin, L. A., *Kinetic Processes in Gases and Molecular Lasers*, Gordon and Breach, London, 1988, Chap. 3.

[25]Aleksandrov, N. L., Konchakov, A. M., and Son, E. E., "Electron Energy Distribution Function and Kinetic Coefficients of a Nitrogen Plasma," *Soviet Journal of Plasma Physics*, Vol. 4, No. 1, 1978, pp. 98–102.

[26]Gorse, C., Paniccia, F., Ricard, A., and Capitelli, M., "Electron Energy Distribution Functions in He–CO Vibrationally Excited Post Discharges," *Journal of Chemical Physics*, Vol. 84, No. 8, 1986, pp. 4717, 4718.

[27]Schlichting, H., *Boundary Layer Theory*, McGraw–Hill, New York, 1960, Chap. 16.

[28]Briley, W. R., and McDonald, H., "Solution of the Multidimensional Compressible Navier–Stokes Equations by a Generalized Implicit Method," *Journal of Computational Physics*, Vol. 24, No. 4, 1977, pp. 372–397.

[29]Gibeling, H. J., and Buggeln, R. C., "Reacting Flow Models for Navier–Stokes Analysis of Projectile Base Combustion," AIAA Paper 91-2077, June 1991.

[30]Babu, V., and Subramaniam, V. V., "Numerical Solutions to Nozzle Flows with Vibrational Nonequilibrium," *Journal of Thermophysics and Heat Transfer*, Vol. 9, No. 2, 1995, pp. 227–232.

[31]Aithal, S. M., and Subramaniam, V. V., "Modeling of Multidimensional Flows with Vibrational Nonequilibrium," AIAA Paper 97-2503, June 1998.

[32]Thomson, J. J., and Thomson, G. P., *Conduction of Electricity Through Gases*, Vol. 1, Cambridge Univ. Press, Cambridge, England, U.K., 1928, Chap. 3.

[33]Adamovich, I., Saupe, S., Grassi, M. J., Shulz. O., Macheret, S., and Rich, J. W., "Vibrationally Stimulated Ionization of Carbon Monoxide in Optical Pumping Experiments," *Chemical Physics*, Vol. 173, No. 3, 1993, pp. 491–504.

[34]Merzkirch, W., *Flow Visualization*, Academic Press, New York, 1974, Chap. 6.

[35]Rich, J. W., "Relaxation of Molecules Exchanging Vibrational Energy," *Applied Atomic Collision Physics*, edited by E. W. McDaniel and W. L. Nighan, Vol. 3, Gas Lasers, Academic Press, New York, 1982, pp. 99–140.

[36]Slovetskii, D. I., *Mechanisms of Chemical Reactions in Nonequilibrium Plasmas*, Nauka, Moscow, 1980, Chap. 4.

[37]Chiroux de Gavelle de Roany, A., Flament, C., Rich, J. W., Subramaniam, V. V., and Warren, W. R., Jr., "Strong Vibrational Nonequilibrium in Supersonic Nozzle Flows," *AIAA Journal*, Vol. 31, No. 1, 1991, pp. 119–238.

[38]Sa, P. A., and Loureiro, J., "A Time-Dependent Analysis of the Nitrogen Afterglow in N_2 and N_2-Ar Microwave Discharges," *Journal of Physics D: Applied Physics*, Vol. 30, No. 16, 1997, pp. 2320–2330.

[39]Adamovich, I. V., Rich, J. W., and Nelson, G. L., "Feasibility Study of Magnetohydrodynamics Acceleration of Unseeded and Seeded Air Flows," *AIAA Journal*, Vol. 36, No. 4, 1998, pp. 590–597.

M. Sichel
Associate Editor